

# Aeroelastic Stability of Composite Hingeless Rotor Blades in Hover—Part I: Theory

M. V. FULTON\* AND D. H. HODGES

School of Aerospace Engineering, Georgia Institute of Technology  
Atlanta, GA, U.S.A.

**Abstract**—A finite-element-based stability analysis is presented for isolated hingeless, composite rotor blades in the hovering flight condition. The formulation is comprised of separate, but compatible, cross-sectional (two-dimensional) and global or beam (one-dimensional) equations. The sectional analyses used account for all possible deformation in the three-dimensional representation of the blade. The global analysis is based on a mixed variational statement for the dynamics of moving beams; it can account for  $6 \times 6$  cross-sectional stiffness and inertia matrices which, respectively, allow for the treatment of shear deformation and rotary inertia. There are no restrictions on the magnitudes of the displacements and rotations if the strain remains small compared to unity. The lift, drag, and pitching moment models are based on two-dimensional, quasi-steady strip theory, with induced inflow taken from momentum theory. The equilibrium operating configuration of the blade is obtained by an iterative solution of the complete nonlinear equations. The dynamic equations are linearized about this position, yielding an eigenproblem. In Part II, numerical results are presented for both extension-twist and bending-twist coupled rotor blades, which indicate that certain “nonclassical” couplings must be included in the analysis in general.

## 1. INTRODUCTION

### 1.1. Background and Motivation

Helicopter rotor aeroelastic stability analyses have become increasingly complicated over the years due to changes in the geometric design and materials used in their construction; see [1]. During the early years of rotor development, designers used articulated rotor blades to provide structural load relief in both the flap and lead-lag directions at the root. In addition, a bearing facilitated rotations about the spanwise axis for pitch changes. The successful design of these mechanisms was an important step towards helicopter flight.

The hinges and bearings of articulated rotors, however, have certain drawbacks. Specifically, these hinges and bearings experience very high local stresses [2] which cause reduced life and, therefore, high maintenance, uncertainty, and cost. In addition, these rotors require the use of lead-lag dampers for stability. These dampers, of course, further increased the maintenance needs, cost, weight, and complexity of the rotor system [1].

Hingeless rotor blades do not have flap or lead-lag hinges, but they may retain the pitch bearing. The many potential advantages of the hingeless rotor, such as simplicity, reduced weight, and potential for improved flying qualities, could not be attained, however, without conquering

---

Based on a paper presented at the 33<sup>rd</sup> Structures, Structural Dynamics and Materials Conference, Dallas, Texas, April 13–15, 1992.

This work was supported by the U.S. Army Research Office under contract DAAL03-89-K-0007 of which Gary L. Anderson was the technical monitor. Technical discussions with Ali R. Atılgan are gratefully acknowledged.

\*Current address: National Research Council, U.S. Army Aeroflightdynamics Directorate, Moffett Field, California.

a significant problem—new aeroelastic instabilities. Moreover, these instabilities could not be adequately predicted by existing rotor stability codes. In response to this challenge, appropriate analytical advances in hingeless rotor stability analysis were made by undertaking new approaches which entailed correctly accounting for geometrically nonlinear blade elastic deformations.

For example, Hodges and Dowell [3] derived equations of motion that are valid for slender, straight, homogeneous, isotropic beams undergoing moderate displacements. Several nonlinear structural and inertial terms in the final equations were identified that can substantially influence the aeroelastic stability of hingeless helicopter rotor blades. The flap-lag-torsion analysis was displacement-based and included no shear deformation. The final, simplified equations of motion were obtained by the use of an “ordering scheme” for associating with each dependent variable an estimated order of magnitude and omitting all terms higher than second order (with some exceptions). The concept of the ordering scheme, though an important method of the time, has been more recently shown to be unnecessary [4].

With this model, for instance, the effects of precone, aerodynamic modeling, and flap-lag structural coupling on stability were investigated. It was shown that flap-lag elastic couplings, along with pitch-lag and pitch-flap couplings induced by geometrically nonlinear blade elastic deformations, noticeably affect stability. Positive precone, for instance, was shown to affect the equilibrium position, thereby modifying the pitch-lag and pitch-flap couplings and adversely affecting stability while reducing equilibrium bending moments as desired [5].

Along with the change in rotor geometric design came changes in the materials. Just as the old wooden blades had given way to metallic blades, so too were metallic blades giving way to composite blades. The reasons were simple and clear: metallic blades were susceptible to corrosion, fatigue, and rapid crack propagation. With the advent of modern composites (such as graphite-epoxy and boron-epoxy), materials were available to overcome the problems inherent in metallic blades. Currently, several rotor designs are hingeless and are manufactured out of composites [2,6].

Another industry-wide change, the development of the tiltrotor aircraft, has provided new challenges for rotor stability analyses. This new challenge exists due to an attempt to optimize the aerodynamic performance of these rotors for both hover and forward flight [7]. One solution to this problem is available through the use of extension-twist coupling. That is, the change in rotor speed from the hover condition to forward flight provides a passive means for changing the rotor blade’s twist distribution.

Both the potential use of blades with elastic couplings (such as extension-twist) and the knowledge that elastic couplings can substantially affect stability call for the development of analyses capable of correctly modeling hingeless composite rotors. Such a development is the subject of this paper.

## 1.2. Previous Work

Composite rotor blade modeling, as defined here, focuses entirely on the structural representation of the blade as exhibited in the cross-sectional elastic constants. [8] describes work done through 1988 in this general area and reveals that such work falls into two categories. Analytical approaches idealize the structural configuration to curved-sided or rectangular closed cells. In these cases, one can extract cross-sectional elastic constants in closed form by following any of several types of approximations, such as an overall restriction to uniaxial stress or a local restriction to include only membrane stresses in the walls. Finite-element-based approaches, on the other hand, allow the modeling of general structural configurations.

The first attempts to model composite rotor blade aeroelastic stability were those of Hong and Chopra [9]. This work modeled the blade as a box beam and, following the isotropic blade analysis of [3], assumed uniaxial stress and suppressed shear deformation. The lack of transverse shear strain led the authors to an analysis that omits both bending-shear and extension-shear couplings.

The orthotropic lamina treatment did, however, permit the inclusion of extension-twist and bending-twist couplings, along with extension-bending and bending-bending couplings. Results seemed to show that dramatically different stability results could be obtained for composite blades, depending on the laminate design of the box beam walls.

While there have been other works since then which have contributed to the modeling of composite blades, very few additional results have been obtained for aeroelastic stability of composite blades until quite recently. When trying to fill this research gap, mentioned by [10], one must remember the recent evidence that transverse shear deformation and “nonclassical” effects such as bending-shear coupling can be important for accurate predictions of composite beam behavior [11]. This implies that a new stability analysis should be developed that incorporates all of these effects; this code should then be validated and used to obtain new insights into composite rotor behavior. We will now discuss a subset of composite blade analyses with the motivation to help the reader understand the present contribution. We will not belabor the exclusively cross-sectional modeling schemes reviewed in [8] except to note a few of those works which are closely related to the present objectives.

The sectional analysis of Giavotto *et al.* [12] was reported by [8] to be the most general extant sectional analysis, and the authors believe that it is still true. Their analysis was recently updated to include initial twist and curvature (see [13]). In principle, this sectional analysis, along with the additional work embodied in [14,15], is capable of modeling completely general composite blades. The only shortcomings are that these analyses do not flow from a common nonlinear three-dimensional analysis and there is no means by which one can assess the error short of comparison with three-dimensional finite element results. No results were presented for aeroelastic stability of composite blades.

In [16] Bauchau and Hong developed a nonlinear, large-displacement analysis for initially curved and twisted composite beams. The analysis represents the finite rotations of the beam by Euler angles; small strain is assumed, along with a uniaxial stress state and moderate initial curvatures. The three necessary three-dimensional strains are augmented by the St. Venant torsional warping function for a thin-walled composite cross-section as reported in [17], and the hoop stress has been neglected akin to [18]. The resulting displacement field is described by seven variables: three translations, three rotations, and one out-of-plane torsional warping sectional “degree of freedom.” The importance of this higher-order out-of-plane deformation is stated to be more significant for composite materials than for isotropic materials. The resulting equations are discretized using four-noded finite elements. Again, no results were presented for aeroelastic stability of composite blades.

Smith and Chopra [19] presented a moderate deflection, finite-element-based analysis for the aeroelastic response and blade loads of composite rotors in forward flight. The blade analysis includes transverse shear deformation and appropriate elastic couplings. The cross-sectional analysis is limited to box beams and is based on [20]. The validation of the analysis is well-documented. As [9,19] demonstrate, a change in the material couplings can modify the damping of the lead-lag mode.

Yuan *et al.* [21] presented a finite-element-based aeroelastic stability analysis for pretwisted, composite rotor blades in the hovering flight condition, including tip sweep and anhedral. The analysis used [22] and [23] as the bases for the kinematics of deformation. The analysis was simplified through the assumption of a uniaxial stress state and restriction to moderate deflections. The displacement field included transverse shear and restrained, out-of-plane torsional warping, which yielded seven variables that describe the behavior of each reference cross-section. These seven measures were stated to be related to the one-dimensional forces through a constitutive law related to that of Kosmatka [24].

Both [19] and [21] do provide aeroelastic stability results. See Part II for additional discussion of these works.

### 1.3. Present Approach

In choosing an appropriate research emphasis in the field of rotor stability, several things should be recognized:

- (1) hingeless (and bearingless) rotors have become and will probably remain popular;
- (2) hingeless rotor stability has been found to be significantly affected by rotor elastic couplings;
- (3) composite materials are widely being used in modern rotor blades; and
- (4) composite materials provide a natural means for aeroelastic tailoring, an example being the extension-twist coupled blades of [7].

In light of the discussion of previous work, where does this leave the state of the art? So far, no aeroelastic stability analyses have been developed which possess all the following characteristics:

- (1) Both sectional and beam analyses follow within *one common framework* from geometrically nonlinear, three-dimensional elasticity, accounting for all possible deformations.
- (2) The sectional analysis is capable of treating *general* composite blades with all possible material couplings accounted for.
- (3) The beam analysis is based on *geometrically exact equations* (i.e., no ordering scheme) so that the only approximations in the analysis arise from the treatment of the structure as a beam (which essentially affects only the accuracy of the one-dimensional constitutive model).

There exists a body of literature, chiefly in the former Soviet Union and the work of Berdichevsky and his co-workers, in which a powerful framework for composite beam analysis is developed. Reference [25] appears to be the first in the literature to plainly state that “the geometrically nonlinear problem of the three-dimensional theory of elasticity for a beam can now be split into a nonlinear one-dimensional problem and a linear two-dimensional problem.” This statement was made concerning homogeneous beams with certain material symmetries. In accordance with this approach, the geometrically nonlinear three-dimensional strain energy of any anisotropic, nonhomogeneous beam is replaced with an asymptotically equivalent one-dimensional strain energy, thus facilitating the derivation of an asymptotically correct constitutive law for a general, anisotropic, nonhomogeneous cross-section. The separation of the three-dimensional problem into two smaller problems (linear cross-sectional (i.e., two-dimensional) and nonlinear global (i.e., one-dimensional) analyses) serves to reduce the computational difficulties associated with general solutions of the complete three-dimensional problem. The method is called the variational-asymptotical method (VAM).

The analysis of [26] presented and applied VAM to arbitrary composite rotor blades. Following the three-dimensional nonlinear kinematical formulation of [27] for small local rotation, the strain energy is written in terms of a  $6 \times 6$  matrix of cross-sectional elastic constants of the same form as that of [12]. For static deformation of composite beams, it was shown that this matrix can be reduced to a  $4 \times 4$  by minimization of the strain energy with respect to the transverse shear strain measures. This is quite different from that which one obtains by simply setting these transverse shear measures equal to zero; this leads to a “classical” theory which is shown to be inadequate for composite rotor blades.

Similarly, [28] uses VAM to develop the  $4 \times 4$  matrix directly for thin-walled composite beams, which can be done only if all possible deformations are included in the three-dimensional representation. Their approach and the one of [26] provide essentially identical stiffnesses for thin-walled beams. Although there are some quantitative differences, stiffnesses from both approaches lead to static deflections and free-vibration frequencies which agree fairly well with those based on the stiffnesses of [12,18].

A strain energy of the form of that from [26] leads directly to the set of equations of motion found in [4], which provides a nonlinear intrinsic formulation for the dynamics of initially curved

and twisted beams in a moving frame. Small strains and local rotations were assumed, but finite rotation of the reference cross-section was represented exactly by Rodrigues parameters. Expressions for the six generalized strain measures were given in terms of the displacement of the reference line and the rotation of the reference cross-section. Next, the nonlinear, intrinsic, one-dimensional dynamic equilibrium equations were developed. These equations include rotary inertia but neglect the kinetic energy associated with cross-sectional warping, which follows naturally from the restriction to small strain. The equations are valid for initially curved and twisted beams with unconstrained warping. For a complete formulation, a material constitutive law was to be taken from the beam's strain energy, which was assumed to be obtainable in terms of the generalized strains alone. The complete formulation was called a "mixed variational formulation," because of the appearance in the governing equations of unknown variables other than displacements or rotations. Use of this formulation with any compatible sectional analysis provides the basis for an aeroelastic stability analysis for composite rotor blades.

In this paper, a composite rotor blade stability analysis based on a finite element solution of the intrinsic, mixed dynamic equations of Hodges [4] is developed. The aerodynamic forces were modeled with two-dimensional quasi-steady strip theory with inflow taken from momentum/blade element theory; the analysis is valid for hingeless, isolated rotor blades in hover. The cross-sectional stiffnesses were taken from codes based on [18,28]. The equilibrium configuration was found in its full, nonlinear form, and the dynamic solution was obtained for small motions about that equilibrium state.

This approach allows for the investigation of composite rotor stability with transverse shear flexibility effects and with complete use of all relevant elastic couplings. With this approach, the adequacy of previous analyses can be tested. In addition, new insights into the behavior of composite beams and rotors can be pursued.

## 2. STRUCTURAL MODEL AND THEORY

It has now been established that, for beams, it is beneficial and feasible to reduce the nonlinear, three-dimensional structural problem to an equivalent problem consisting of two separate parts:

- (1) a linear, two-dimensional cross-sectional analysis, and
- (2) a nonlinear, one-dimensional global analysis.

In this section, the blade model will be described, along with all of the accompanying theory. For the notations and geometrical descriptions used in this work, see [4,27,29]. First, the *linear, two-dimensional cross-sectional analysis* will be discussed. Afterwards, the *nonlinear one-dimensional global analysis* will be presented. Finally, some simplifying assumptions will be described.

### 2.1. Cross-Sectional Analysis

This section addresses the linear, two-dimensional cross-sectional analysis through (1) its formulation, and (2) various solution strategies.

#### 2.1.1. Formulation

The results obtained in [30] are compatible with the assumption by [4] and others that a function of the form

$$U = U(\gamma, \kappa) \quad (1)$$

can be found or suitably approximated, where  $\gamma(x_1)$  and  $\kappa(x_1)$  are the intrinsic strain measures given by

$$\gamma \triangleq \begin{Bmatrix} \gamma_{11} \\ 2\gamma_{12} \\ 2\gamma_{13} \end{Bmatrix}, \quad \kappa \triangleq \begin{Bmatrix} \kappa_1 \\ \kappa_2 \\ \kappa_3 \end{Bmatrix}. \quad (2)$$

The column matrix  $\gamma$  contains the three strain measures at  $x_2 = x_3 = 0$ ;  $\gamma_{11}$  is the extensional strain, while  $2\gamma_{12}$  and  $2\gamma_{13}$  are transverse shear strains. Similarly, the column matrix  $\kappa$  contains the three curvatures due to deformation;  $\kappa_1$  is the elastic twist per unit length, while  $\kappa_2$  and  $\kappa_3$  are the elastic bending curvatures.

In addition, [4] stipulates that if two column matrices are defined so that

$$\begin{aligned} F &\triangleq \begin{Bmatrix} F_1 \\ F_2 \\ F_3 \end{Bmatrix} = \left( \frac{\partial U}{\partial \gamma} \right)^\top, \\ M &\triangleq \begin{Bmatrix} M_1 \\ M_2 \\ M_3 \end{Bmatrix} = \left( \frac{\partial U}{\partial \kappa} \right)^\top, \end{aligned} \quad (3)$$

then the previous choice for  $\gamma$  and  $\kappa$  implies that  $F(x_1)$  is the resultant force acting on the cross-section at the reference line:  $F_1$  is the axial force, while  $F_2$  and  $F_3$  are the shear forces. In addition,  $M(x_1)$  is the resultant moment:  $M_1$  is the torsion moment, while  $M_2$  and  $M_3$  are the bending moments.

The relation between  $F$ ,  $M$ ,  $\gamma$ , and  $\kappa$ , which is compatible with equation (1), can be written as

$$\begin{Bmatrix} F \\ M \end{Bmatrix} = \begin{bmatrix} A & B \\ B^T & D \end{bmatrix} \begin{Bmatrix} \gamma \\ \kappa \end{Bmatrix}, \quad (4)$$

where  $A$ ,  $B$ , and  $D$  are  $3 \times 3$  matrices of constants that can be calculated once for each cross-section. (Note that these matrices should not be confused with those of plate theory.)

There is a nonlinear effect on the torsional stiffness which is nonnegligible for thin-walled, open cross-sections, sometimes known as the trapeze effect. This phenomenon was modeled herein using the approach of [31]; additional theoretical details can be found in [32]. More specifically, the  $D_{11}$  of equation (4) was obtained by using the formula

$$D_{11} = (D_{11})_{\text{material}} + \left( \frac{D_{22} + D_{33}}{A_{11}} \right) \bar{F}_1, \quad (5)$$

where  $\bar{F}_1$  is the equilibrium value of the axial force, whose coefficient reduces to the polar moment of inertia divided by the cross-sectional area for isotropic cases. In general, the  $6 \times 6$  stiffness matrix is not only a function of the cross-section's material distribution and geometry, but also of the local curvature and twist of the beam.

### 2.1.2. Solution strategies

The above discussion basically reduces to the following question: Can a given cross-section's stiffness characteristics be calculated? For the most general strategies, three things must be known in order to perform this calculation:

- (1) the cross-section's geometry,
- (2) the cross-section's material distribution, and
- (3) the initial twist and curvature of the beam at the cross-section under consideration.

If these three things are known, various methods can be used to calculate the stiffness matrix of equation (4). As previously discussed, two principal solution techniques include (1) an analytical approach, and (2) a numerical approach.

The analysis of [18] was implemented in a computer program, TAIL, written by Mark Nixon. This program vividly demonstrates the power of analytical methods. Specifically, the results obtained by TAIL are very good for thin, closed, single cells, and are very easily and quickly generated; see [33]. The approach employed by TAIL is sufficient for situations in which the load bearing members of the blade can be accurately modeled with thin-walled approximations.

Another program ATWCS (Anisotropic Thin-Walled Closed Section—written by Ashraf Badir) is based on the analytically-based method of [28]. ATWCS has all of the advantages of TAIL plus being asymptotically exact. For more general configurations, however, other approaches need to be used.

Finite element methods provide the modeling generality needed for arbitrary section geometry and material distribution. For example, a finite element implementation of [12] was designed and written by Marco Borri and his co-workers; it is called NABSA—Nonhomogeneous Anisotropic Beam Section Analysis. In addition, VABS (Variational Asymptotical Beam Sectional analysis), was written by Carlos E. S. Cesnik and based upon [26]. The principal advantages of codes like NABSA and VABS is their tremendous versatility. Because of its highly developed finite element library, NABSA's only limitations are computer storage capacity and run time.

In [34], all four cross-sectional codes were used as appropriate. In Part II of this paper, however, only TAIL and ATWCS stiffnesses were used.

## 2.2. Global Analysis

With both the one-dimensional strain energy of equation (1) and the corresponding constitutive relation of equation (4) having been established, it is now appropriate to discuss the global analysis. The discussion will begin with a general description of the mixed variational formulation; it will conclude with the solution strategy used in this work.

### 2.2.1. Mixed variational formulation

The global analysis is based upon the mixed variational formulation of [4]. In this paper, the weak form of all the governing equations was written as

$$\begin{aligned}
& \int_{t_1}^{t_2} \int_0^\ell \left\{ \left[ \left( \overline{\delta q} \right)^\top - \overline{\delta q}^\top \tilde{K} - \overline{\delta \psi}^\top (\tilde{e}_1 + \tilde{\gamma}) \right] F + \left[ \left( \overline{\delta \psi'} \right)^\top - \overline{\delta \psi}^\top \tilde{K} \right] M \right. \\
& \quad - \left( \overline{\delta \dot{q}}^\top - \overline{\delta \dot{q}}^\top \tilde{\Omega} - \overline{\delta \dot{\psi}}^\top \tilde{V} \right) P - \left( \overline{\delta \dot{\psi}}^\top - \overline{\delta \dot{\psi}}^\top \tilde{\Omega} \right) H \\
& \quad + \delta \gamma^\top \left[ \left( \frac{\partial U}{\partial \gamma} \right)^\top - F \right] + \delta \kappa^\top \left[ \left( \frac{\partial U}{\partial \kappa} \right)^\top - M \right] - \delta V^\top \left[ \rho (V - \tilde{\xi} \Omega) - P \right] \\
& \quad - \delta \Omega^\top (I \Omega + \rho \tilde{\xi} V - H) + \overline{\delta f}^\top \left[ e_1 + \tilde{k} u - C^\top (e_1 + \gamma) \right] - \left( \overline{\delta F'} \right)^\top u \\
& \quad - \overline{\delta P}^\top (v + \tilde{\omega} u - C^\top V) + \overline{\delta \dot{P}}^\top u + \overline{\delta M}^\top \left( \Delta + \frac{\tilde{\theta}}{2} + \frac{\theta \theta^\top}{4} \right) (Ck - k - \kappa) - \left( \overline{\delta M'} \right)^\top \theta \\
& \quad - \overline{\delta H}^\top \left( \Delta + \frac{\tilde{\theta}}{2} + \frac{\theta \theta^\top}{4} \right) (C\omega - \Omega) + \overline{\delta \dot{H}}^\top \theta - \overline{\delta q}^\top f - \overline{\delta \psi}^\top m \left. \right\} dx_1 dt \\
& = - \int_0^\ell \left( \overline{\delta q}^\top \hat{P} + \overline{\delta \psi}^\top \hat{H} - \overline{\delta P}^\top \hat{u} - \overline{\delta H}^\top \hat{\theta} \right) \Big|_{t_1}^{t_2} dx_1 \\
& \quad + \int_{t_1}^{t_2} \left( \overline{\delta q}^\top \hat{F} + \overline{\delta \psi}^\top \hat{M} - \overline{\delta F}^\top \hat{u} - \overline{\delta M}^\top \hat{\theta} \right) \Big|_0^\ell dt,
\end{aligned} \tag{6}$$

where the column matrices  $F$ ,  $M$ ,  $\gamma$ , and  $\kappa$  are as previously defined. Other quantities of interest include the following column matrices whose elements are the measure numbers of the indicated vectors (in the undeformed,  $b$ , or deformed,  $B$ , basis): the curvature vector for the undeformed beam (in the  $b$  basis),  $k$ ; the curvature vector for the deformed beam (in the  $B$  basis),  $K = k + \kappa$ ; the displacement of the reference line (in the  $b$  basis),  $u$ ; Rodrigues parameters (relating the  $b$  and  $B$  bases),  $\theta$ ; the angular velocity of the undeformed beam cross-sectional frame (in the  $b$  basis),  $\omega$ ; the velocity of the undeformed beam reference line (in the  $b$  basis),  $v$ ; the angular velocity of

the deformed beam cross-sectional frame (in the  $B$  basis),  $\Omega$ ; the velocity of the deformed beam reference line (in the  $B$  basis),  $V$ ; the section angular momentum (in the  $B$  basis),  $H$ ; the section linear momentum (in the  $B$  basis),  $P$ ; the associated measures of virtual displacement, virtual rotation, etc.; the position of the section mass center relative to the beam reference line (in the  $B$  basis),  $\xi$ ; the section inertia matrix (in the  $b$  basis for the undeformed beam, which is the same as that of the deformed beam in the  $B$  basis since warping is ignored in the inertial operator),  $I$ ; the distributed applied force per unit length (in the  $B$  basis),  $f$ ; and the distributed applied moment per unit length (in the  $B$  basis),  $m$ . Finally,  $\ell$  is the blade's length;  $\rho$  is the blade's mass per unit length; the  $\hat{(\ )}$  (hat) quantities are boundary terms; the mark  $\tilde{(\ )}$  denotes a cross-product operator;  $e_1 = [1\ 0\ 0]^T$ ; and  $\Delta$  is the identity matrix. (For additional details, see [4].)

### 2.2.2. Solution strategy

As stated in the introduction, the goal of the present paper is to provide an analysis to calculate the stability of various rotor configurations that are tailored through the use of composite materials. The linear stability results can be obtained by linearization of the dynamics of the blade about its nonlinear equilibrium configuration, which is an adequate measure of stability, provided that the dynamic motions are small in some sense.

In this work, the linear dynamics were calculated by assuming that the time dependence is completely captured by a complex exponential factor. This method permits decaying, steady, or growing oscillatory motions. To begin this formulation, the temporal integral of equation (6) should be removed; prior to doing this, however, the time derivatives are removed from  $\overline{\delta q}$ ,  $\overline{\delta \psi}$ ,  $\overline{\delta P}$ , and  $\overline{\delta H}$  by integrating the appropriate terms by parts. This operation will shift the time derivatives to  $P$ ,  $H$ ,  $u$ , and  $\theta$ , respectively, along with adding new temporal boundary conditions. The time integral and all of the temporal boundary conditions can now be removed, resulting in

$$\begin{aligned}
\int_0^\ell \left\{ \left[ \left( \overline{\delta q'} \right)^\top - \overline{\delta q}^\top \tilde{K} - \overline{\delta \psi}^\top (\tilde{e}_1 + \tilde{\gamma}) \right] F + \left[ \left( \overline{\delta \psi'} \right)^\top - \overline{\delta \psi}^\top \tilde{K} \right] M \right. \\
+ \overline{\delta q}^\top \left( \dot{P} + \tilde{\Omega} P \right) + \overline{\delta \psi}^\top \tilde{V} P + \overline{\delta \psi}^\top \left( \dot{H} + \tilde{\Omega} H \right) \\
+ \delta \gamma^\top (A \gamma + B \kappa - F) + \delta \kappa^\top (B^\top \gamma + D \kappa - M) \\
- \delta V^\top (\rho V - P) - \delta \Omega^\top (I \Omega - H) \\
+ \overline{\delta F}^\top \left[ e_1 + \tilde{k} u - C^\top (e_1 + \gamma) \right] - \left( \overline{\delta F'} \right)^\top u \\
- \overline{\delta P}^\top (v + \tilde{\omega} u - C^\top V) - \overline{\delta P}^\top \dot{u} \\
+ \overline{\delta M}^\top \left( \Delta + \frac{\tilde{\theta}}{2} + \frac{\theta \theta^\top}{4} \right) (C k - k - \kappa) - \left( \overline{\delta M'} \right)^\top \theta \\
- \overline{\delta H}^\top \left( \Delta + \frac{\tilde{\theta}}{2} + \frac{\theta \theta^\top}{4} \right) (C \omega - \Omega) - \overline{\delta H}^\top \dot{\theta} \\
\left. - \overline{\delta q}^\top f - \overline{\delta \psi}^\top m \right\} dx_1 = \left( \overline{\delta q}^\top \hat{F} + \overline{\delta \psi}^\top \hat{M} - \overline{\delta F}^\top \hat{u} - \overline{\delta M}^\top \hat{\theta} \right) \Big|_0^\ell,
\end{aligned} \tag{7}$$

where the constitutive law of equation (4) has been used. For the cases analyzed in Part II, we also assume that  $\tilde{\xi} = 0$  so that the undeformed beam reference line passes through the cross-sectional mass centers. Note that this assumption may not be suitable for some sectional analysis programs which require a particular choice of the reference line.

### Finite element discretization

With only a spatial integral remaining in equation (7), the beam can now be divided into  $N$  one-dimensional elements of equal length, resulting in  $N + 1$  nodes, with  $f$ ,  $m$ ,  $v$ , and  $\omega$  constant

within each element. Spatial shape functions, valid within each element, can now be chosen for each virtual quantity and dependent variable. Although shape functions of many different types are permissible, the integration will be simplified by choosing the simplest shape functions possible. With this in mind, we let the spatially differentiated quantities be taken to be linear, with all remaining variables being constant within each element [4]. The resulting equations are still nonlinear and contain the unknowns  $u, \theta, \gamma, \kappa, F, M, V, \Omega, P,$  and  $H,$  along with  $\dot{u}, \dot{\theta}, \dot{P},$  and  $\dot{H},$  for each element. (For additional details, see [35]).

Even though the above choice of “crude” shape functions might be thought to lead to long computer run times, they actually produce a code that runs quite well (approximately 90 seconds of CPU time on a Sun-4 for both the equilibrium and the eigen-solution with  $N = 16$ ). In addition, these simple functions, which facilitate the use of symbolic manipulation in writing the code, allow for element quadrature by inspection and produce algebraic equations which are tremendously sparse—a characteristic which is exploited.

### Nonlinear equilibrium equations

The differential set of equations obtained by the finite element discretization can now be put into a more suitable form by separating the solution into two parts:

- (1) equilibrium, and
- (2) dynamic.

This separation is performed by letting each unknown,  $(\quad)$ , be written as a sum of its equilibrium value,  $(\bar{\quad})$ , plus its dynamic value,  $(\check{\quad})$ , such as

$$y(t) = \bar{y} + \check{y}e^{\lambda t}, \quad (8)$$

where  $y$  is some dependent variable and  $\lambda$  is complex. This substitution implies that  $\dot{u} = \lambda \check{u}e^{\lambda t}$ , with analogous relations for  $\dot{\theta}, \dot{P},$  and  $\dot{H}.$

After these substitutions have been performed for each element and all terms have been expanded, the equilibrium equations can be formulated by dropping all terms containing  $(\check{\quad})$  terms. The resulting equations will be nonlinear algebraic equations which can be solved by a standard Newton-Raphson method.

The Newton-Raphson technique, of course, requires the factorization of the Jacobian at each increment of the solution. Our Jacobian, produced when using the simple shape functions described above, is very sparse. This sparsity was exploited by using a sparse matrix linear equation solver, MA28, that is included in the Harwell numerical library [36]. In addition to exploiting sparsity, this subroutine can also save the decomposition pattern of a matrix. This technique produces computational savings when a matrix is given to MA28 that duplicates the sparsity pattern of a previously decomposed matrix—a common occurrence during Newton-Raphson iterations.

### Linear dynamic equations

The equilibrium solution can now be considered to be known. Specifically, all equilibrium terms analogous to  $\bar{y}$  in equation (8) are known, and the equations governing the dynamic (or check) terms can be formulated. The formulation will be based upon dynamic equations that are linearized about the nonlinear equilibrium.

To formulate these dynamic equations, take the product of the Jacobian of the equilibrium equations and the dynamic column matrix, denoted by  $\check{Y}$ ; add the terms arising from the  $\dot{u}, \dot{\theta}, \dot{P},$  and  $\dot{H}$  terms of equation (7), and set this sum equal to zero. Now partition  $\check{Y}$  into two submatrices,  $\check{x}_d$  and  $\check{x}_s$ ; let the variables that have time derivatives be grouped into  $\check{x}_d,$  and group all of the remaining variables into  $\check{x}_s.$  With this grouping, the equation governing the beam dynamics becomes

$$\begin{bmatrix} A_c & B_c \\ C_c & D_c \end{bmatrix} \begin{Bmatrix} \check{x}_d \\ \check{x}_s \end{Bmatrix} = \lambda \begin{bmatrix} 0 & 0 \\ F_c & 0 \end{bmatrix} \begin{Bmatrix} \check{x}_d \\ \check{x}_s \end{Bmatrix}, \quad (9)$$

where  $A_c$ ,  $B_c$ ,  $C_c$ ,  $D_c$ , and  $F_c$  are known, constant matrices that are functions of the equilibrium position. This matrix equation can be ultimately reduced to

$$-\lambda (B_c D_c^{-1} F_c) \dot{x}_d = (A_c - B_c D_c^{-1} C_c) \dot{x}_d, \quad (10)$$

where the assembly of equation (9) was designed such that  $D_c$  would be nonsingular in equation (10).

The above linear equation can be solved as an eigenproblem. Specifically, the IMSL FORTRAN subroutine DVCRG was used for calculating the complex eigenvalues (each of which contains a modal frequency and damping) and their corresponding complex eigenvectors for these small motions about the nonlinear equilibrium position.

### 2.3. Simplifying Assumptions

Thus far, the theory presented has been kept largely generic in order to facilitate future research. Here, however, the equations will be restricted by adopting certain assumptions with regards to the blade's geometry. Specifically, the blade is taken to be a cantilevered beam with root offset, precone, and constant initial twist, operating in hover. First, the kinetics and kinematics of this simple blade will be described. Next, the boundary conditions will be discussed. Finally, various forcing functions will be defined.

#### 2.3.1. Rotor blade kinetics and kinematics

As previously mentioned, the reference line,  $r$ , was chosen such that it passes through the undeformed beam's mass centers, giving  $\bar{\xi} = 0$ . In addition,  $\mathbf{b}_2$  and  $\mathbf{b}_3$  were chosen to be parallel to the principal axes, reducing  $I$  to a diagonal matrix.

In addition, the beam's undeformed geometry is known and fixed relative to a reference frame,  $a$ , whose motion is known relative to inertial space. The frame  $a$  is now defined such that it is stationary except for some angular velocity with respect to inertial space,  $\omega^{ai}$ , so that  $\omega^{ai} = \omega_{a3} \mathbf{a}_3$ , where  $\mathbf{a}_3$  is chosen to be vertically upward and  $\omega_{a3}$  is constant. Finally, choose  $\mathbf{a}_1$  and  $\mathbf{a}_2$  to complete the orthonormal, right-handed reference triad. (See Figure 1.)

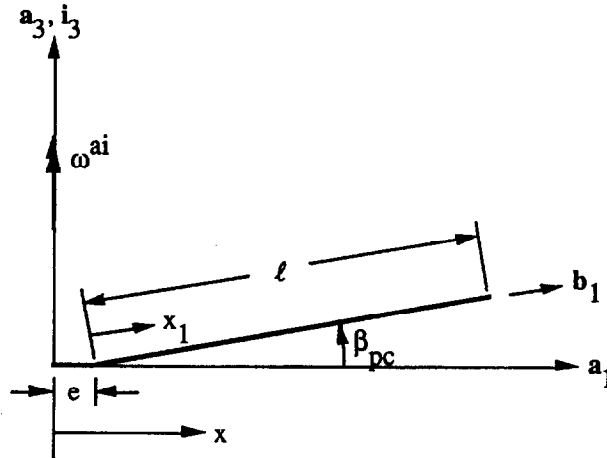


Figure 1. Schematic of rotor (side view).

The reference frame  $b$  will now be chosen so as to permit constant initial twist,  $k_1$ , but no initial curvature (i.e.,  $k_2 = k_3 = 0$ ). In addition, the beam will be allowed to have both initial precone,  $\beta_{pc}$ , and a hinge offset,  $e$ . With  $e$  specified, the position vector to the root of  $r$  becomes  $\mathbf{r}|_{x_1=0} = e\mathbf{a}_1$ . The complete description of  $k_1$  and  $\beta_{pc}$ , however, requires the specification of several direction cosine matrices.

To begin, let  $\mathbf{b}_i = \mathbf{a}_i$  if  $\beta_{pc} = k_1 = 0$ . Now, define a new frame  $q$  that is related to  $a$  by a rotation of magnitude  $\beta_{pc}$  about  $-\mathbf{a}_2$ . Specifically, if  $\mathbf{q}_i = C_{ij}^{qa} \mathbf{a}_j$  (note that repeated indices are summed from 1 to 3), then

$$C^{qa} = \begin{bmatrix} \cos \beta_{pc} & 0 & \sin \beta_{pc} \\ 0 & 1 & 0 \\ -\sin \beta_{pc} & 0 & \cos \beta_{pc} \end{bmatrix}. \quad (11)$$

In the most general case,  $b$  differs from  $q$  by a rotation  $\theta_p(x_1)$  about  $\mathbf{q}_1$ . As before, if  $\mathbf{b}_i = C_{ij}^{bq} \mathbf{q}_j$ , then

$$C^{bq} = \begin{bmatrix} 1 & 0 & 0 \\ 0 & \cos \theta_p & \sin \theta_p \\ 0 & -\sin \theta_p & \cos \theta_p \end{bmatrix}. \quad (12)$$

With the above groundwork completed, the column matrix  $k$  can now be represented as

$$k = \begin{Bmatrix} \theta'_p \\ 0 \\ 0 \end{Bmatrix}, \quad (13)$$

where

$$\theta_p = (\theta_p)_0 + x_1 k_1, \quad (14)$$

with  $(\theta_p)_0 = \theta_p|_{x_1=0}$  being the blade's "root pitch angle," and with  $k_1 = \theta'_p$  being a constant.

If equation (11) is substituted into equation (12), and if  $\mathbf{b}_i = C_{ij}^{ba} \mathbf{a}_j$ , then

$$C^{ba} = \begin{bmatrix} \cos \beta_{pc} & 0 & \sin \beta_{pc} \\ -\sin \theta_p \sin \beta_{pc} & \cos \theta_p & \sin \theta_p \cos \beta_{pc} \\ -\cos \theta_p \sin \beta_{pc} & -\sin \theta_p & \cos \theta_p \cos \beta_{pc} \end{bmatrix}. \quad (15)$$

Since  $\omega^{ai} = \omega_{a3} \mathbf{a}_3$ , the column matrix  $\omega$  can now be written in terms of  $\theta_p$  and  $\beta_{pc}$  by noting that  $\omega_i = \omega_{a3} C_{i3}^{ba}$ . Specifically,

$$\omega = \omega_{a3} \begin{Bmatrix} \sin \beta_{pc} \\ \sin \theta_p \cos \beta_{pc} \\ \cos \theta_p \cos \beta_{pc} \end{Bmatrix}. \quad (16)$$

In addition, the column matrix  $v$  contains the measure numbers in  $b$  of the velocity of  $r$  in an inertial frame,  $\mathbf{v}^{b^*i}$ , where

$$\mathbf{v}^{b^*i} = \omega^{bi} \times \mathbf{r}, \quad (17)$$

and  $\mathbf{r}$  represents the position vector from  $O$  of frame  $a$  to points on  $r$ , such that  $\mathbf{r} = e\mathbf{a}_1 + x_1\mathbf{b}_1$ ; the use of  $C_{i1}^{ba}$  leads to

$$\mathbf{r} = (x_1 + e \cos \beta_{pc}) \mathbf{b}_1 - (e \sin \theta_p \sin \beta_{pc}) \mathbf{b}_2 - (e \cos \theta_p \sin \beta_{pc}) \mathbf{b}_3. \quad (18)$$

Now equation (17) can be written in matrix form as

$$v = \begin{bmatrix} 0 & -\omega_3 & \omega_2 \\ \omega_3 & 0 & -\omega_1 \\ -\omega_2 & \omega_1 & 0 \end{bmatrix} \begin{Bmatrix} x_1 + e \cos \beta_{pc} \\ -e \sin \theta_p \sin \beta_{pc} \\ -e \cos \theta_p \sin \beta_{pc} \end{Bmatrix}, \quad (19)$$

where  $\omega_i = \omega^{bi} \cdot \mathbf{b}_i$  as found in equation (16). Simplification of equation (19) produces

$$v = \omega_{a3} (x_1 \cos \beta_{pc} + e) \begin{Bmatrix} 0 \\ \cos \theta_p \\ -\sin \theta_p \end{Bmatrix}. \quad (20)$$

### 2.3.2. Boundary conditions

The boundary conditions for a cantilevered beam are quite straightforward. For instance, let the beam be fixed at the root of the beam ( $x_1 = 0$ ) and free at its tip ( $x_1 = \ell$ ). With this choice, it is well-known that the displacements and rotations are zero at the root, while the forces and moments at the tip are determined by the applied tip loads. These boundary conditions can be represented mathematically as

$$\begin{aligned}\hat{u}_{(1)} &= 0, \\ \hat{\theta}_{(1)} &= 0,\end{aligned}\tag{21}$$

and

$$\begin{aligned}\hat{F}_{(N+1)} &= \hat{F}_g, \\ \hat{M}_{(N+1)} &= \hat{M}_g,\end{aligned}\tag{22}$$

where  $\hat{F}_g$  and  $\hat{M}_g$  are the *given* concentrated tip force and moment, respectively, both equal to zero for typical stability problems.

### 2.3.3. Forcing functions

All of the forcing functions enter the equations for the  $i^{\text{th}}$  element through some combination of

- (1) the distributed force per unit length,  $f_{(i)}$ ,
- (2) the distributed moment per unit length,  $m_{(i)}$ ,
- (3) the concentrated tip forces,  $\hat{F}_{(i)}$  and  $\hat{F}_{(i+1)}$ , and
- (4) the concentrated tip moments,  $\hat{M}_{(i)}$  and  $\hat{M}_{(i+1)}$ .

For a tip mass, the force exerted on the beam by gravity should be represented as a ‘‘constant dead force.’’ An additional force, however, arises when the mass accelerates. This inertial force can be modeled by reformulating the kinetic energy used to derive equation (6). This modification, however, is not necessary since all of the characteristics of the tip mass can be captured by slight modifications of the previously formed governing equations.

Specifically, the tip mass can be represented by a short, undeformable finite element. In this way, the inertial properties of the tip mass can be modeled and additional variables that describe the motion of the tip mass can be introduced. To appropriately modify the governing equations, set  $\gamma_{(N)} = 0$  and  $\kappa_{(N)} = 0$ , where  $N$  is the element number corresponding to the last element. In addition, since the last element is now rigid, remove the six scalar equations that define the constitutive law for this element. The resulting set of governing equations will now automatically account for the inertial reactions arising from the acceleration of the tip mass.

## 3. AERODYNAMIC MODEL AND THEORY

It is becoming increasingly accepted that advanced aerodynamic modeling is important for accurately predicting the stability of hingeless rotors under all operating conditions. The effects of nonlinear aerodynamics, dynamic stall, and dynamic inflow are all important in various flight and stability regimes. These effects, however, are considered to be secondary to the principal emphasis of this work. That is, the modifications in stability characteristics obtainable from elastic couplings, along with the evaluation of the structural portion of current stability analyses, is not nullified by these refined aerodynamic effects. Although these effects are important, the goals of the present paper can be met without their inclusion.

For the above reasons, a two-dimensional, quasi-steady lift theory is used. The inflow is based upon momentum/blade element theory. This inflow is assumed to remain at its equilibrium value during the blade’s small motions about the equilibrium position.

The quasi-steady lift is obtained by use of the two-dimensional, steady lift-curve slope, along with the instantaneous angle of attack. This lift, along with the corresponding drag and pitching

moment, is taken about the aerodynamic center of the airfoil and includes both circulatory and noncirculatory terms. For offsets between the aerodynamic center and  $x_2 = x_3 = 0$ , appropriate transformations are made to find the relative wind velocity, at the aerodynamic center, in terms of the cross-section's generalized velocities and the inflow; finally, the resulting aerodynamic forces and moment are transformed back to  $x_2 = x_3 = 0$ .

### 3.1. Aerodynamic Lift, Drag, and Moment

The aerodynamic lift, drag, and moment equations are those which give the magnitude and direction of the aerodynamic forces in terms of the relative wind velocity. To begin, it will be helpful to develop some notation. First, let the aerodynamic force acting on the aerodynamic center of the blade be designated by  $\mathbf{F}_a^Q$ , where point  $Q$  is the aerodynamic center of the airfoil (see Figure 2). Similarly, the aerodynamic moment about  $Q$  is designated by  $\mathbf{M}_a^Q$ . Next, let  $Z$  be the "airfoil coordinate system" whose center is placed at  $Q$ ;  $\mathbf{Z}_2$  and  $\mathbf{Z}_3$  are in the plane of the airfoil, with  $\mathbf{Z}_2$  parallel to the zero-lift line and directed towards the airfoil's leading edge. We define the relationship between  $\mathbf{Z}_i$  and  $\mathbf{B}_i$  in terms of a rotation of magnitude  $\alpha_a$  about  $\mathbf{B}_1 = \mathbf{Z}_1$ , such that

$$C^{ZB} = \begin{bmatrix} 1 & 0 & 0 \\ 0 & \cos \alpha_a & \sin \alpha_a \\ 0 & -\sin \alpha_a & \cos \alpha_a \end{bmatrix}. \tag{23}$$

Another coordinate system, the "wind coordinate system," is represented as  $W$  and is identical to  $Z$  except for a rigid rotation by the angle of attack  $\alpha$  as shown in Figure 2. Finally, represent the position vector from  $B^*$  (the origin of  $B$ ) to  $Q$  as  $\mathbf{p}^{Q/B^*} = p_2 \mathbf{B}_2 + p_3 \mathbf{B}_3$ .

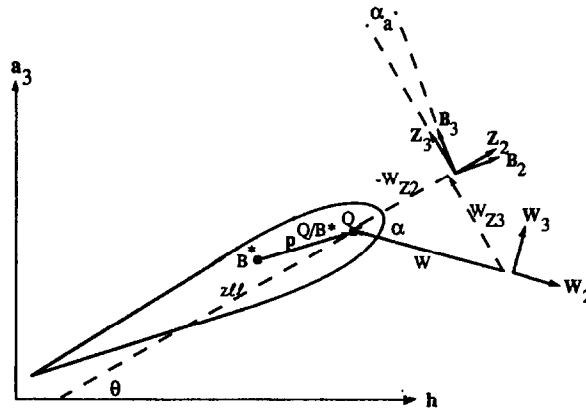


Figure 2. Schematic of airfoil (looking towards the root of the blade).

Now, the aerodynamic force and moment at  $B^*$  are easily calculated as

$$\begin{aligned} \mathbf{F}_a^{B^*} &= \mathbf{F}_a^Q, \\ \mathbf{M}_a^{B^*} &= \mathbf{M}_a^Q + \mathbf{p}^{Q/B^*} \times \mathbf{F}_a^Q, \end{aligned} \tag{24}$$

with

$$\begin{aligned} \mathbf{F}_a^Q &= L_c \mathbf{W}_3 - D \mathbf{W}_2 + L_{nc} \mathbf{Z}_3, \\ \mathbf{M}_a^Q &= M_a \mathbf{B}_1, \end{aligned} \tag{25}$$

where  $\mathbf{F}_a^{B^*}$  and  $\mathbf{M}_a^{B^*}$  are the aerodynamic components of  $\mathbf{f}$  and  $\mathbf{m}$ , the total applied loads acting on the beam; more specifically,  $\mathbf{f} = f_i \mathbf{B}_i = \mathbf{F}_a^{B^*} + \dots$  and  $\mathbf{m} = m_i \mathbf{B}_i = \mathbf{M}_a^{B^*} + \dots$ , where the dots signify affects of forces of other than aerodynamic origin. The symbols  $L_c$ ,  $D$ ,  $L_{nc}$ , and  $M_a$  denote, respectively, the circulatory lift, drag, noncirculatory lift, and moment as given in Kunz

and Hodges [37]:

$$\begin{aligned}
L_c &= \frac{1}{2}\rho_\infty W^2 c c_l + \frac{\pi}{2}\rho_\infty c^2 W G, \\
D &= \frac{1}{2}\rho_\infty W^2 c c_d, \\
M_a &= \frac{1}{2}\rho_\infty W^2 c^2 c_m - \frac{\pi}{16}\rho_\infty c^3 \left( W G + \dot{W}_{Z3} + \frac{3c}{8}\dot{G} \right), \\
L_{nc} &= \frac{\pi}{4}\rho_\infty c^2 \left( \dot{W}_{Z3} + \frac{c}{4}\dot{G} \right),
\end{aligned} \tag{26}$$

where  $\rho_\infty$  is the air density;  $c$  is the chord;  $W$  is the relative speed of the wind in the plane of the airfoil,  $G$  is the flow velocity gradient, and  $W_{Z3}$  is the flow velocity normal to the zero-lift line; and  $c_l$ ,  $c_d$ , and  $c_m$  are the lift, drag, and moment coefficients, respectively, each being a function of  $\alpha$ , the angle of attack. Note that equation (26) was determined in [37] by the use of a quasi-steady adaptation of Greenberg's thin-airfoil theory [38].

### 3.2. Relative Wind

If  $\mathbf{V}^Q$  is the inertial velocity of point  $Q$  (the aerodynamic center) and  $\boldsymbol{\nu}$  is the inflow for the radial station which corresponds to  $Q$ , then the relative wind vector can be represented as

$$\mathbf{W} = -\mathbf{V}^Q + \boldsymbol{\nu}, \tag{27}$$

where

$$\begin{aligned}
\mathbf{V}^Q &= \mathbf{V} + \boldsymbol{\Omega} \times \mathbf{p}^{Q/B^*}, \\
\boldsymbol{\nu} &= -\nu \mathbf{a}_3.
\end{aligned} \tag{28}$$

If  $\mathbf{V}^Q = U_i \mathbf{Z}_i$  and it is recognized that  $\mathbf{a}_3 = C_{3i}^{aZ} \mathbf{Z}_i$ , then the components of  $\mathbf{W}$  in the plane of the airfoil section become

$$\begin{aligned}
W_{Z2} &= \mathbf{W} \cdot \mathbf{Z}_2 = -U_2 - \nu C_{32}^{aZ}, \\
W_{Z3} &= \mathbf{W} \cdot \mathbf{Z}_3 = -U_3 - \nu C_{33}^{aZ},
\end{aligned} \tag{29}$$

where

$$\begin{aligned}
U_2 &= (V_2 - \Omega_1 p_3) \cos \alpha_a + (V_3 + \Omega_1 p_2) \sin \alpha_a, \\
U_3 &= -(V_2 - \Omega_1 p_3) \sin \alpha_a + (V_3 + \Omega_1 p_2) \cos \alpha_a,
\end{aligned} \tag{30}$$

and  $C^{aZ}$  can be found from

$$C^{aZ} = C^{ab} C^\top C^{BZ}. \tag{31}$$

Finally, the flow velocity gradient, whose general definition is

$$G = -\frac{\partial W_{Z3}}{\partial (p_2 \cos \alpha_a + p_3 \sin \alpha_a)} \tag{32}$$

can be simply expressed as

$$G = \Omega_1. \tag{33}$$

### 3.3. Inflow

The inflow is calculated using the following equation from [39]:

$$\nu = \omega_{a3} R \left( \frac{\sigma a}{16} \right) \left[ -1 + \sqrt{1 + \frac{32x\theta}{\sigma a R}} \right], \tag{34}$$

where  $R$  is the radius of the rotor,  $\sigma$  is the solidity,  $a$  is the lift-curve slope,  $x$  is the minimum distance from the  $\mathbf{a}_3$  axis to the point of interest, and  $\theta$  is the angle between the zero-lift line and the rotor's plane of rotation (see Figure 2).

To calculate  $\theta$ , let  $\mathbf{h} = C_{21}^{Za} \mathbf{a}_1 + C_{22}^{Za} \mathbf{a}_2$  represent the projection of  $\mathbf{Z}_2$  (the zero-lift line unit vector) in the  $\mathbf{a}_1$ - $\mathbf{a}_2$  plane (i.e., the "plane of rotation"). Introduction of the rule of dot products

$$\mathbf{Z}_2 \cdot \mathbf{h} = |\mathbf{Z}_2| |\mathbf{h}| \cos \theta \quad (35)$$

leads to

$$\theta = \cos^{-1} \left[ \sqrt{(C_{21}^{ZA})^2 + (C_{22}^{ZA})^2} \right] \text{sign}(C_{23}^{Za}). \quad (36)$$

The sign of  $\theta$  was determined based on the orientation of  $\mathbf{Z}_2$ : if the  $\mathbf{a}_3$  component of  $\mathbf{Z}_2$  is positive, then the airfoil is pitched nose up; the sign of  $\theta$  can therefore be determined by the sign of  $C_{23}^{Za}$  since  $\mathbf{Z}_2 \cdot \mathbf{a}_3 = C_{23}^{Za}$ .

The remaining quantities needed to calculate the inflow are

$$\begin{aligned} x &= \sqrt{(\mathbf{R} \cdot \mathbf{a}_1)^2 + (\mathbf{R} \cdot \mathbf{a}_2)^2}, \\ R &= [x]_{x_1=\ell}, \\ \sigma &= \frac{bc}{\pi R}, \end{aligned} \quad (37)$$

where  $\mathbf{R}$  is the position vector from point  $O$  (typically the center of rotation) to a point on the deformed reference line and  $b$  equals the number of rotor blades.

### 3.4. Lift, Drag, and Moment Coefficients

For the purpose of generating the results in Part II, the coefficient of lift,  $c_l$ , is related to the angle of attack by the equation

$$c_l = a \sin \alpha = a \frac{W_{Z3}}{\sqrt{W_{Z2}^2 + W_{Z3}^2}}, \quad (38)$$

where  $\alpha$  is the angle of attack;  $\sin \alpha > 0$  when  $W_{Z3} > 0$ . The drag coefficient is taken to be a constant, such that  $c_d = c_{d0}$ . Finally, the pitching moment coefficient is assumed to be zero.

## 4. DISCUSSION AND CONCLUDING REMARKS

A finite-element-based stability analysis has been presented for isolated hingeless, composite rotor blades in the hovering flight condition. The formulation is comprised of separate, but compatible, cross-sectional (two-dimensional) and global or beam (one-dimensional) equations. The weak form of all the beam governing equations is used as the basis for the present analysis; these equations are in mixed form, so called because unknowns include quantities other than displacements and rotations. These weak, mixed equations include the intrinsic equations of motion, as well as constitutive and kinematical equations, for the dynamics of initially curved and twisted beams in a moving frame [4]. The constitutive equations are valid for the case of small strain and small local rotation [27]. Otherwise, there are no explicit restrictions on the magnitudes of the beam's displacement and rotation; that is, the beam analysis is geometrically exact. The formulation includes the effects of rotary inertia and assumes that a strain energy function in terms of certain one-dimensional strain variables is given. In keeping with this strain energy assumption, a symmetric  $6 \times 6$  sectional stiffness matrix, which relates the one-dimensional forces and moments to the strains and elastic curvatures, was used in the representation of the beam's strain energy. The components of this stiffness matrix were calculated using various linear cross-sectional analyses, some of which are capable of treating general composite blades with all

possible material couplings accounted for, with the specific analysis being chosen as appropriate for each situation.

For the purpose of generating the results given in Part II, the aerodynamic forces are calculated using quasi-steady strip theory with inflow taken from momentum/blade element theory. The analysis is specialized for spanwise uniform blades with zero initial curvature, constant pretwist, root offset, and a precone angle; additional configuration detail was included in the derivations to clarify the implementation of the beam formulation used in this work.

For solving the equations for aeroelastic stability, one-dimensional finite elements were used to discretize the weak form of the governing equations of motion. The resulting mixed method, along with the use of simple shape functions, permits element quadrature by inspection, which facilitate the use of symbolic manipulation in writing the code. The resulting nonlinear ordinary differential equations in time were solved by separating the solution into two parts: a constant equilibrium value plus a small dynamic value. Numerical solution of the resulting nonlinear equilibrium solution was performed by using the Newton-Raphson technique. Symbolic manipulation was used to generate the Jacobian and residual needed by the Newton-Raphson method, and factorization of the Jacobian was performed using a sparse matrix routine. The dynamics are governed by equations linearized about the equilibrium solution. The solution of the resultant eigenproblem includes both complex eigenvalues (modal frequencies and dampings) and the corresponding complex eigenvectors for these small dynamic motions. Validation and composite blade stability results are given in Part II.

## REFERENCES

1. R.A. Ormiston, Investigations of hingeless rotor stability, *Vertica* **7** (2), 143–181 (1983).
2. B. Kelley, Helicopter evolution, *Journal of the American Helicopter Society* **28** (1), 3–9 (1983).
3. D.H. Hodges and E.H. Dowell, Nonlinear equations of motion for the elastic bending and torsion of twisted nonuniform rotor blades, NASA TN D-7818, (1974).
4. D.H. Hodges, A mixed variational formulation based on exact intrinsic equations for dynamics of moving beams, *International Journal of Solids and Structures* **26** (11), 1253–1273 (1990).
5. D.H. Hodges and R.A. Ormiston, Stability of elastic bending and torsion of uniform cantilever rotor blades in hover with variable structural coupling, NASA TN D-8192, (1976).
6. R.L. Foye and J.L. Shipley, Evolution of the application of composite materials to helicopters, *Journal of the American Helicopter Society* **26** (4), 5–15 (1981).
7. M.W. Nixon, Extension-twist coupling of composite circular tubes with application to tilt rotor blade design, *Proceedings of the 28<sup>th</sup> Structures, Structural Dynamics, and Materials Conference*, Paper No. 87-0772, Monterey, CA, (April 6–8, 1987).
8. D.H. Hodges, Review of composite rotor blade modeling, *AIAA Journal* **28** (3), 561–565 (1990).
9. C.H. Hong and I. Chopra, Aeroelastic stability analysis of a composite rotor blade, *Journal of the American Helicopter Society* **30** (2), 57–67 (1985).
10. P.P. Friedmann, Helicopter rotor dynamics and aeroelasticity: Some key ideas and insights, *Vertica* **14** (1), 101–121 (1990).
11. L.W. Rehfield, A.R. Atilgan and D.H. Hodges, Nonclassical behavior of thin-walled composite beams with closed cross-sections, *Journal of the American Helicopter Society* **35** (2), 42–50 (1990).
12. V. Giavotto, M. Borri, P. Mantegazza and G. Ghiringhelli, Anisotropic beam theory and applications, *Computers and Structures* **16** (1–4), 403–413 (1983).
13. M. Borri, G.L. Ghiringhelli and T. Merlini, Linear analysis of naturally curved and twisted anisotropic beams, *Composites Engineering* **2** (5–7), 433–456 (1992).
14. M. Borri and P. Mantegazza, Some contributions on structural and dynamic modeling of rotor blades, *L'Aerotecnica Missili e Spazio* **64** (9), 143–154 (1985).
15. M. Borri and T. Merlini, A large displacement formulation for anisotropic beam analysis, *Meccanica* **21** (1), 30–37 (1986).
16. O.A. Bauchau and C.H. Hong, Large displacement analysis of naturally curved and twisted composite beams, *AIAA Journal* **25** (11), 1469–1475 (1987).
17. O.A. Bauchau, A beam theory for anisotropic materials, *Journal of Applied Mechanics* **52** (2), 416–422 (1985).
18. L.W. Rehfield, Design analysis methodology for composite rotor blades, Presented at the 7<sup>th</sup> DoD/NASA Conference on Fibrous Composites in Structural Design, Paper No. AFWAL-TR-85-3094, pp. (V(a)-1)–(V(a)-15), Denver, CO, (June 17–20, 1985).

19. E.C. Smith and I. Chopra, Aeroelastic response and blade loads of a composite rotor in forward flight, *Proceedings of the 33<sup>rd</sup> Structures, Structural Dynamics, and Materials Conference*, Paper No. 92-2466-CP, Dallas, TX, (April 13–17, 1992).
20. E.C. Smith and I. Chopra, Formulation and evaluation of an analytical model for composite box-beams, *Journal of the American Helicopter Society* **36** (3), 22–35 (1991).
21. K.A. Yuan, P.P. Friedmann and C. Venkatesan, A new aeroelastic model for composite rotor blades with straight and swept tips, *Proceedings of the 33<sup>rd</sup> Structures, Structural Dynamics, and Materials Conference*, Paper No. 92-2259-CP, Dallas, TX, (April 13–17, 1992).
22. G. Wempner, *Mechanics of Solids with Applications to Thin Bodies*, Sijthoff & Noordhoff, Rockville, MD, (1981).
23. K. Washizu, Some considerations on a naturally curved and twisted slender beam, *Journal of Mathematics and Physics* **43** (2), 111–116 (1964).
24. J.B. Kosmatka, Structural dynamic modeling of advanced composite propellers by the finite element method, Ph.D. Dissertation, Mechanical, Aerospace, and Nuclear Engineering Department, University of California, Los Angeles, (1986).
25. V.L. Berdichevsky, On the energy of an elastic rod, *PMM* **45** (4), 518–529 (1981).
26. D.H. Hodges, A.R. Atilgan, C.E.S. Cesnik and M.V. Fulton, On a simplified strain energy function for geometrically nonlinear behavior of anisotropic beams, *Composites Engineering* **2** (5–7), 513–526 (1992).
27. D.A. Danielson and D.H. Hodges, Nonlinear beam kinematics by decomposition of the rotation tensor, *Journal of Applied Mechanics* **54** (2), 258–262 (1987).
28. V.L. Berdichevsky, E.A. Armanios and A. Badir, Theory of anisotropic thin-walled closed-cross-section beams, *Composites Engineering* **2** (5–7), 411–432 (1992).
29. D.A. Danielson and D.H. Hodges, A beam theory for large global rotation, moderate local rotation, and small strain, *Journal of Applied Mechanics* **55** (1), 179–184 (1988).
30. A.R. Atilgan, D.H. Hodges, M.V. Fulton and C.E.S. Cesnik, Application of the variational-asymptotical method to static and dynamic behavior of elastic beams, *Proceedings of the 32<sup>nd</sup> Structures, Structural Dynamics, and Materials Conference*, Paper No. 91-1026, Baltimore, MD, (April 8–10, 1991).
31. L.W. Rehfield and A.R. Atilgan, On the buckling behavior of thin-walled laminated composite open section beams, *Proceedings of the 30<sup>th</sup> Structures, Structural Dynamics, and Materials Conference*, Paper No. 89-1171, Mobile, AL, (April 3–5, 1989).
32. D.H. Hodges and A.R. Atilgan, Asymptotical modeling of initially curved and twisted composite rotor blades, *Proceedings of the American Helicopter Society International Technical Specialists' Meeting on Rotorcraft Basic Research*, Paper No. 47, Atlanta, GA, (March 25–27, 1991).
33. R.V. Hodges, M.W. Nixon and L.W. Rehfield, Comparison of composite rotor blade models: A coupled-beam analysis and an MSC/NASTRAN finite-element model, NASA TM 89024, (1987).
34. M.V. Fulton, Stability of elastically tailored rotor blades, Ph.D. Dissertation, School of Aerospace Engineering, Georgia Institute of Technology, Atlanta, GA, (1992).
35. D.H. Hodges, A.R. Atilgan, M.V. Fulton and L.W. Rehfield, Free-vibration analysis of composite beams, *Journal of the American Helicopter Society* **36** (3), 36–47 (1991).
36. I.S. Duff, Harwell Subroutine Library, Computer Science and Systems Division, Harwell Laboratory, Oxfordshire, England, (February 1988).
37. D.L. Kunz and D.H. Hodges, Analytical modeling of helicopter static and dynamic induced velocity in GRASP, *Vertica* **12** (4), 337–344 (1988).
38. J.M. Greenberg, Airfoil in sinusoidal motion in a pulsating stream, NACA TN 1326, (1947).
39. A. Gessow and G.C. Myers, *Aerodynamics of the Helicopter*, Eighth printing, p. 68, College Park Press, Bethesda, MD, (1985).